

Integrated Computer Wind Design for Bridge Engineering

Johann STAMPLER
Senior Project Engineer
TDV GmbH,
Graz, Austria
office@tdv.at

Johann Stampler, born 1951, civil engineering degree from the Technical University of Civil Engineering, Graz. Over 30 years of experience in structural analysis in a wide range of applications.

Dorian JANJIC
Managing Director
TDV GmbH,
Graz, Austria
office@tdv.at

Dorian Janjic, born 1960, civil engineering degree from the Faculty of Civil Engineering, Sarajevo. 15 years of experience in technical research, software development.

Andreas DOMAINGO
CFD Engineer
TDV GmbH,
Graz, Austria
office@tdv.at

Andreas Domaingo, born 1977, PhD degree in technical physics from the Technical University of Graz 2005. Currently working as CFD engineer with TDV.

Summary

In the design process of long-span bridges the consideration of wind effects is a major point because the extraordinary slenderness of these structures yields a considerable susceptibility for wind-induced vibrations. Usually, extensive wind tunnel tests are performed to investigate the aerodynamic behaviour of such structures. Due to increasing computer power, numerical CFD methods are becoming a serious alternative at much lower costs. In the framework of the research project *NUWIMOD*, a discrete vortex method was integrated into the structural analysis program *RM2006*. This strong coupling of structural analysis and CFD calculation provides an opportunity for fast and comprehensive investigation of wind effects. In this paper, aspects of the wind analysis performed for the Hardanger fjord bridge project are presented.

Keywords: Wind impact, wind buffeting, Hardanger bridge, aerodynamic coefficients, computational fluid dynamics (CFD), discrete vortex method, wind tunnel tests.

1. Introduction

At least since the wind-induced collapse of the first Tacoma Narrows bridge in 1940 it is known that great emphasis must be put on the interaction of long span bridges and wind. Although the Navier-Stokes equations, which provide a physical model to describe the air flow, are known since the first half of the 19th century, it was not possible to solve these equations for the complicated bridge deck cross sections for a long time. The main source for aerodynamic coefficients were expensive wind tunnel tests. With the development of computers, it was for the first time possible to calculate real world problems. Since then, two major solution techniques have evolved: methods which rely on a computational grids and grid-free methods.

Grid-free methods treat the Navier-Stokes equations in a Lagrangian manner, i.e. the position of particles is tracked in time. These methods are usually termed as discrete vortex methods (DVM). First attempts to apply this method were made in the 1930s by Rosenhead. In the following the basic idea was continuously improved concerning accuracy and computation time, the last point obviously supported by the explosion of computer power in the last decade. In the 1970s and 80s, the main interest, when applying vortex methods, was to calculate the flow around airfoils. First applications of DVM methods to bridge decks were reported in the early 90s, because other CFD models so far available proved to be of too high computational effort which is a clear disadvantage in the day-to-day usage. Vortex methods were applied successfully for the calculation of many bridge decks in the last years, cf. for example [1-3]. In this sense, they can be seen as a powerful tool for accelerating the construction process of long span bridges.

The research project *NUWIMOD* aims at the integration of a DVM method into *TDV's* structural analysis program *RM2006* and the application to long span bridges like the Hardanger bridge. The advantage of such an integrated approach is that no complicated import and export of the structure geometry and resulting data between the CFD and structural analysis parts are necessary. Any change in any part is immediately accessible for the other one without further complications. This is

of particular interest for engineers interested in an all-in-one solution. Moreover a feedback of the structural response to wind-induced forces into the running CFD calculation is possible. A flow chart for integrated and non-integrated solutions is presented in Figs. 1 and 2.

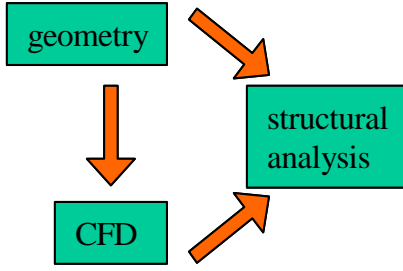


Fig. 1 Flow chart of non-integrated solution.

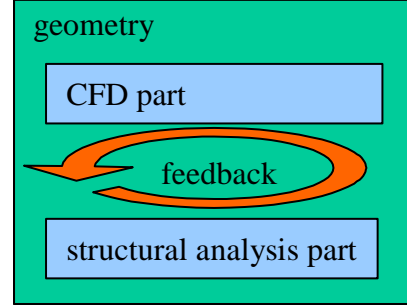


Fig. 2 Flow chart of integrated solution.

2. Discrete Vortex Method

The Discrete Vortex Method is applied to solve the vorticity transport equation (VTE) for 2D cross sections governing the time evolution of the vorticity field ω

$$\frac{\partial \omega}{\partial t} + (\mathbf{u} \cdot \nabla) \omega = \nu \nabla^2 \omega, \quad \omega = \nabla \times \mathbf{u} \quad (1)$$

where \mathbf{u} denotes the velocity and ν is the kinematic viscosity of air. It can be derived from the Navier-Stokes equations for incompressible fluids at constant temperature. The boundary conditions (b.c.) are chosen such that the oncoming velocity far away from the cross section is prescribed. Along the surface of the cross section, one demands either a vanishing normal component of the velocity (no penetration b.c.) or a vanishing tangential component (no slip b.c.).

The vorticity field ω is represented by a large number of vortex particles of given size σ and circulation Γ located at positions \mathbf{x}_i :

$$\omega(\mathbf{x}) = \sum_i \delta_\sigma(\mathbf{x} - \mathbf{x}_i) \Gamma_i, \quad (2)$$

where δ_σ is a Dirac-Delta like core function of spread σ . The surface of the cross section is approximated by straight panels, which are associated with a linearly varying surface vorticity γ . The velocity boundary condition along the surface together with the global conservation of circulation can be used to determine this surface vorticity, which is subsequently diffused into the flow as new vortex particles.

The time integration of (1) is performed by applying an operator splitting method. The first fractional step treats the convection term on the left hand side. Here the characteristics of the vortex particles are tracked in a Lagrangian manner, and a first order Euler scheme or second order Runge-Kutta scheme can be applied. The velocity is reconstructed from the vorticity field via the Biot-Savart relation

$$u(\mathbf{x}) = U_\infty - \int \frac{\omega(\mathbf{x}_0) \times (\mathbf{x}_0 - \mathbf{x})}{|\mathbf{x}_0 - \mathbf{x}|^2} d\mathbf{x}_0, \quad (3)$$

where U_∞ denotes the wind velocity. The diffusion term on the right hand side is handled by a random walk method.

3. Investigated bridge

The Hardanger bridge in Norway will cross the Hardanger fjord to replace the ferry transport (cf. Fig. 3). The main span length will be 1310 m at a total length of 1380 m. The bridge will be the longest suspension bridge in Norway and no 7 worldwide. A *RM2006* structural model of the bridge

is shown in Fig. 4.



Fig. 3 Location of Hardanger bridge.



Fig. 4 Structural model of Hardanger bridge.

The small difference of main length to span arises, because the shore drops very steeply into the fjord. Compared to the huge span of the bridge, the dimensions of the main girder cross sections are only approximately 18.3 x 3.2 m. This makes the bridge very susceptible to wind-effects and a careful investigation of wind effects becomes even more important.

4. CFD calculation

4.1 Aerodynamic investigation of main girder

The main girder of the Hardanger bridge will be located about 53 m above ground level. At this height, a nominal wind velocity of 38 m/s can be expected. For the present study two variations of the girder were considered: once the plain girder and once with attached wind guiding vanes and spoilers. The cross section is shown in Fig. 5, where the red parts mark additional vanes and spoilers, and the parameters are given in Tab. 1.

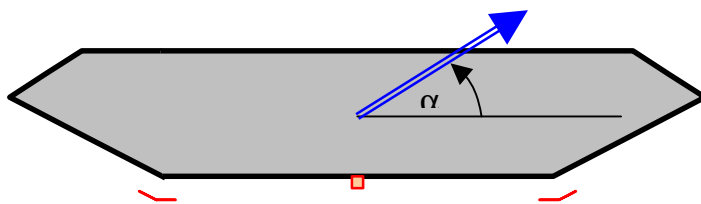


Fig. 5 Simplified cross section of main girder with definition of attack angle α .

Tab. 1 Model parameters.

Height H	3.18	m
Width B	18.30	m
Density of mass of air	1.25	kg/m ³
Kinematic viscosity	1.5×10^{-5}	m ² /s

CFD calculations were performed for three different parameter configurations:

- at a Reynolds number $Re = 10^5$ (lRe) and cross section without spoilers
- at a Reynolds number $Re = 5.5 \times 10^7$ (hRe), which corresponds to the nominal velocity, and cross section without spoilers
- at a Reynolds number $Re = 5.5 \times 10^7$ (hRe, S) with guiding vanes and spoilers

Additionally, the calculation results were compared with a wind tunnel test (wt) with a 1:100 model of the cross section without guiding vanes and spoilers at a Reynolds number $Re = 10^5$.

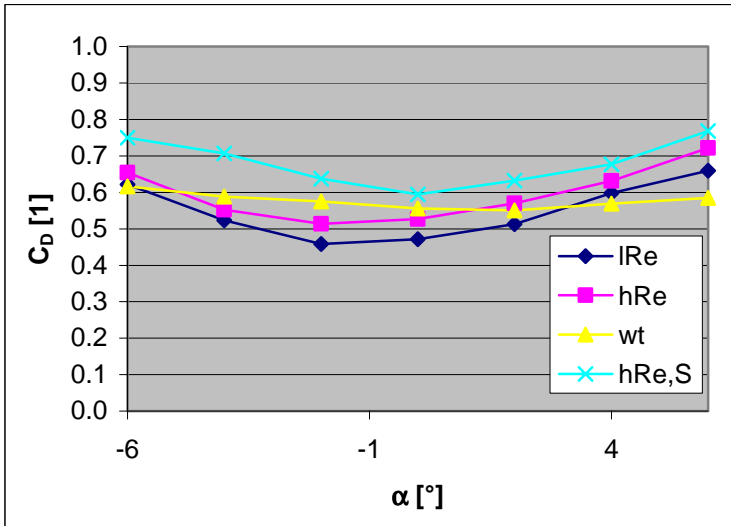


Fig. 6 Drag coefficients for main girder cross section in dependence of attack angle α .

considering an effective increase of the height of the cross section due to the guiding vanes and spoilers (cf. Fig. 5), they cause only small changes of the drag coefficient.

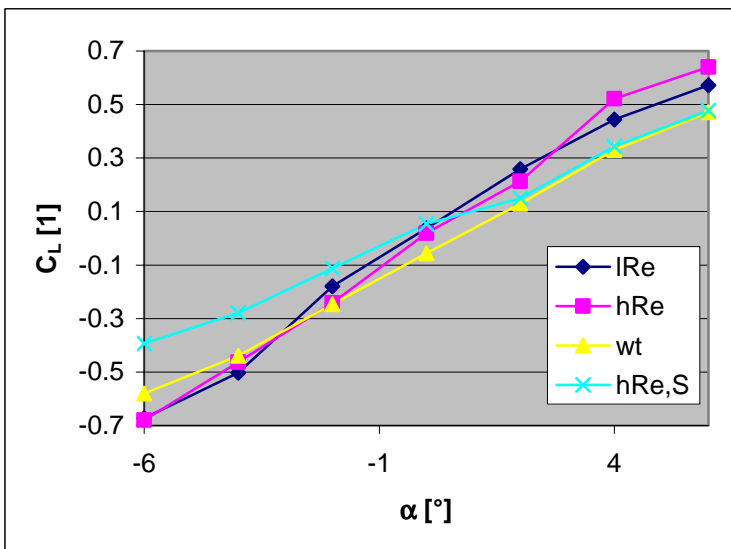


Fig.7 Lift coefficients for main girder cross section in dependence of attack angle α .

Fig. 6 shows the drag coefficient for an attack angle between -6° and 6° for the four different cases.

Only a low dependency of the drag coefficient on the Reynolds number could be observed. Compared to the wind tunnel test, the calculated drag coefficients display a stronger dependency on the attack angle, but the general agreement is good. The drag coefficient $C_D(\alpha = 0^\circ) \approx 0.5$ is in good agreement with other cross sections of the same shape (cf. for example [1]).

In the case of attached wind guiding vanes an increased drag coefficient was observed. It should be noted that the same normalisation length H was used for all CFD calculations. By considering an effective increase of the height of the cross section due to the guiding vanes and spoilers (cf. Fig. 5), they cause only small changes of the drag coefficient.

The lift coefficient is presented in Fig.7. Again, almost no Reynolds number dependency is predicted by the CFD calculation.

The application of wind guiding vanes and spoilers leads to decreased lift coefficients for increasing absolute values of the attack angle. Due to the additional obstacles, the periodic separation of large vortices is disturbed and the flow becomes more turbulent. This reduced vortex shedding can also be observed by considering the power spectra of lift and moment coefficient. Comparisons for the cross section with and without spoilers are shown in Fig. 8 for the lift coefficient and in Fig. 9 for the moment coefficient. The pronounced peaks at low frequencies are replaced by small peaks distributed over

several frequencies, which reduces the risk of flutter, because less energy is dissipated at certain frequencies.

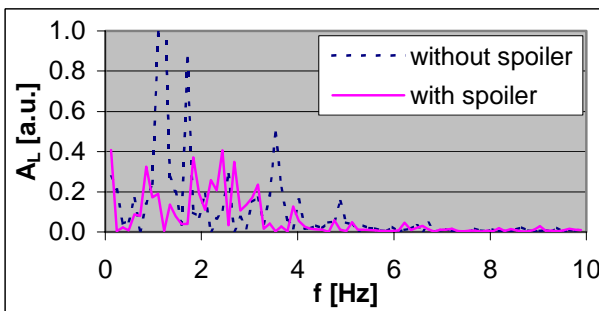


Fig. 8 Power spectrum of lift coefficient

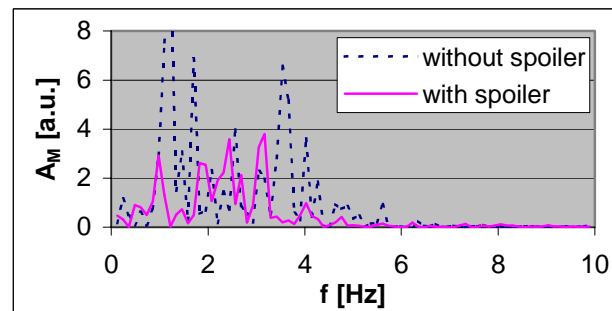


Fig. 9 Power spectrum of moment coefficient.

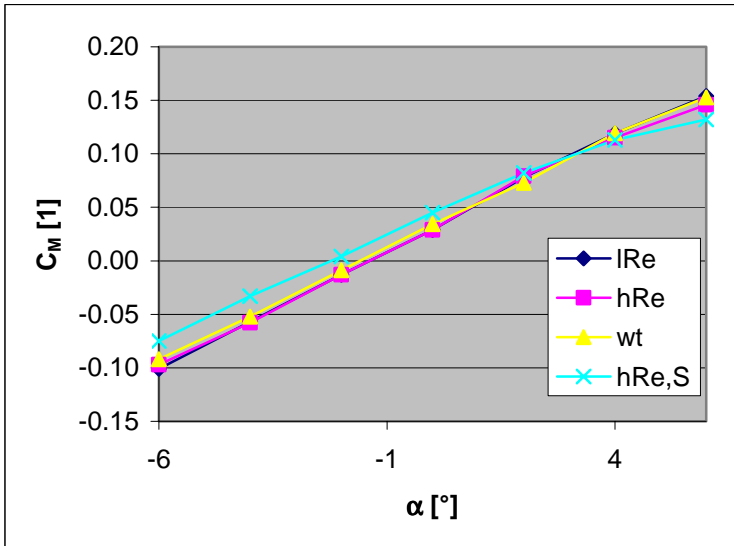


Fig. 10 Moment coefficients for main girder cross section.

4.2 Aerodynamic investigation of pylons

The pylon legs are modelled by two rectangles with an aspect ratio of the sides $H:B = 4:3$ and a reference length $H = 6$ m. The distance S between the centres of the legs depends on the height above ground. Considered distances are approximately 15 m, 20 m and 25 m. A sketch of the geometry is shown in Fig. 11. Although the basic elements of the cross section have been intensively reported in the literature, a detailed insight into the aerodynamic behaviour of a dual bluff body is usually not given. In the present study, wind directions from 0° to 90° at Reynolds numbers above 10^7 were considered.

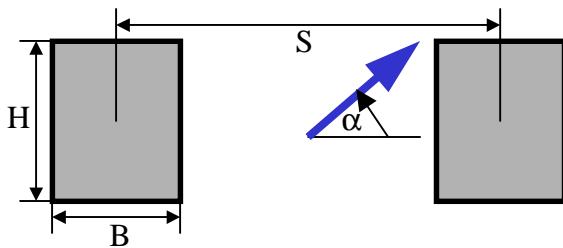


Fig. 11 Considered pylon geometry.

For low attack angles $\alpha \approx 0^\circ$, the right leg lies in the wind shadow of the left one. Consequently a significantly reduced drag coefficient can be expected for transversal wind. For longitudinal wind direction, $\alpha \approx 90^\circ$, it is not clear a priori, if the distance between the legs is small enough to cause interactions between the two legs.

The results of the performed CFD calculations are presented in Fig. 12 for the drag coefficients. All coefficients were normalised with respect to the height H of a leg.

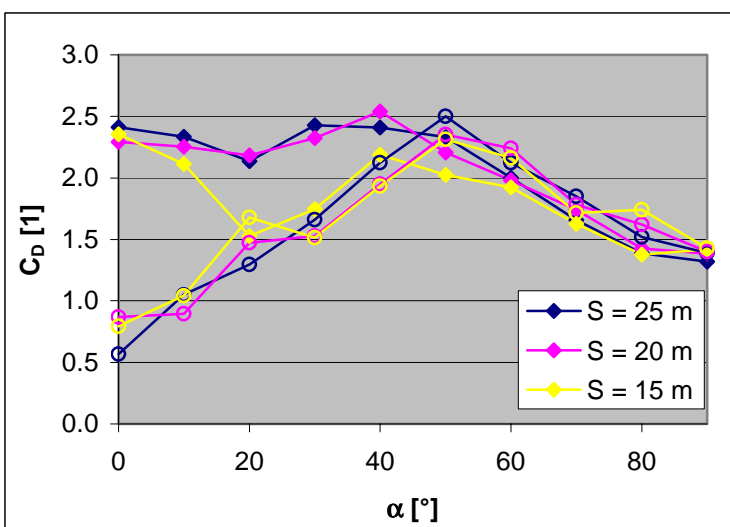


Fig. 12 Drag coefficient C_D of left (\blacklozenge) and right (\circ) pylon leg in dependence of attack angle for different distances S .

Finally, the moment coefficient is shown in Fig. 10. In this case, no Reynolds number dependency could be observed and there is a very good agreement between CFD calculations and wind tunnel experiments.

If wind guiding vanes and spoilers are present, a reduction of the moment coefficient can be expected for angles $|\alpha| > 2^\circ$. For small angles, the CFD calculations revealed a small increase.

As expected, strong wind shadow effects of the drag coefficient can be observed for lateral wind directions. For longitudinal incidence, the pylon geometry is symmetric with respect to the wind direction, which is also reflected by the drag coefficient. In general, for angles $\alpha > 45^\circ$, the coefficients for both legs show a good agreement.

For the considered geometry, the two legs are "seen" well separated by the oncoming flow for angles $\alpha > 30^\circ$. Consequently, one can differ between

three regions. In the first region up to 30° , the right leg is completely or partially in the wind shadow of the left one. Here, the drag coefficient of the left leg decreases and the one of the right leg increases with increasing angle. In the region between 30° and 45° , the right leg is still partially in the wake of the left leg. The drag of both legs increases in this region. In general, only a small influence of the distance between the pylon legs can be observed, except at $\alpha = 20^\circ$, where the drag coefficient is much smaller if the legs come very close to each other.

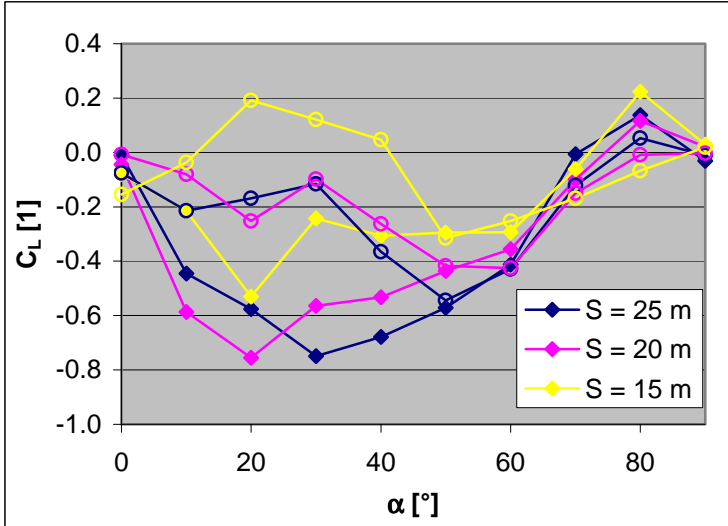


Fig. 13 Lift coefficient C_L of left (\blacklozenge) and right (\circ) pylon leg in dependence of attack angle for different distances S .

situation could be observed, because there exists a region for the attack angle $20^\circ < \alpha < 40^\circ$, where the lift coefficient changes sign compared to the other cases. A possible explanation are strong interactions of the wakes behind the two legs.

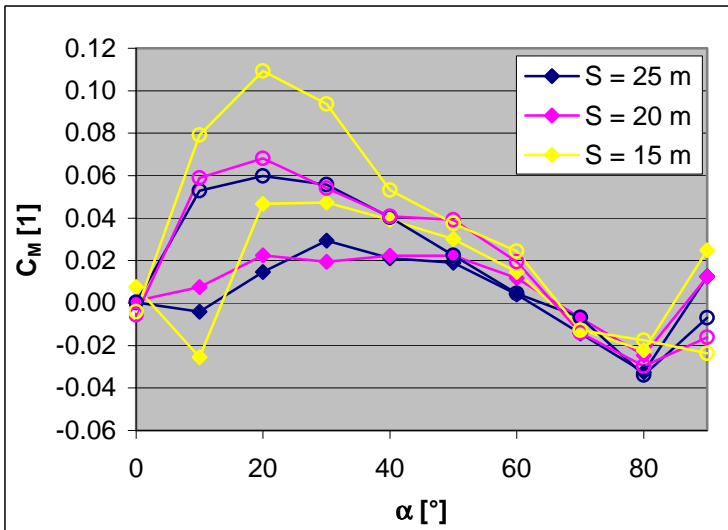


Fig. 14 Moment coefficient C_M of left (\blacklozenge) and right (\circ) pylon leg as function of angle for different distances S .

explained by an unbalanced ratio of drag and lift forces due to wind shadow effects.

5. Summary

With the increasing number of long span bridges being constructed all over the world, the aerodynamic investigation of bridge deck cross sections or whole bridges is a topic of actual interest. The increasing computer power makes the numerical treatment of such investigations feasible. By

The lift coefficients for the two legs are shown in Fig. 13. In this case, it must be distinguished between the coefficients for different distances. If the legs are separated by a distance greater than 20 m, the coefficients for the both legs are almost the same for angles greater than 45° , which could already be observed for the drag coefficient. For lower angles, the same qualitative behaviour of the lift coefficient is predicted, however less regular in the case that the distance between the legs becomes smaller.

If the distance becomes even smaller, the dependence of the lift coefficient on the angle shows only small similarities with the ones for greater distances, if the left leg is considered.

For the right leg, a completely new situation could be observed, because there exists a region for the attack angle $20^\circ < \alpha < 40^\circ$, where the lift coefficient changes sign compared to the other cases. A possible explanation are strong interactions of the wakes behind the two legs.

Similar observations as for the lift coefficient can be made for the moment coefficient, which is presented in Fig. 14. For attack angles $\alpha > 45^\circ$, there is a good agreement of the coefficients of the two legs. For longitudinal wind, $\alpha = 90^\circ$, the moment coefficients of the right leg have nearly the opposite sign as the ones for the left leg, which conforms well with symmetry considerations.

For small angles, there is a good agreement of the coefficients for distances $S = 25$ m and $S = 20$ m, as for the lift coefficient, and a noticeable deviation, if the distance becomes smaller. Compared to the lift coefficient, it can be noted, that the moment coefficient of the right leg is higher for small angles, which can be explained by an unbalanced ratio of drag and lift forces due to wind shadow effects.

combining CFD codes with structural analysis programs, a considerable gain of time during the design process is possible.

In the present paper, we have presented a discrete vortex method which has been implemented in the structural analysis program RM2006. Two examples were discussed: First, the comparison of wind tunnel data with CFD computations for a bridge deck, where a good agreement was observed. And second, the investigation of a free standing pylon with a discussion of wind shadow effects.

6. Acknowledgements

The authors gratefully acknowledge that the work for this paper was funded by the FFG on behalf of the Austrian Government and by the SFG on behalf of the province of Styria as part of the research project NUWIMOD.

7. References

- [1] WALTHER, J.H., *Discrete Vortex Method for Two-Dimensional Flow past Bodies of Arbitrary Shape Undergoing Prescribed Rotary and Translational Motion*, PhD Thesis, Technical University of Denmark, Lyngby, 1994.
- [2] MORGENTHAL, G., *Aerodynamic Analysis of Structures Using High-resolution Vortex Particle Methods*, PhD Thesis, University of Cambridge, Cambridge, 2002.
- [3] LARSEN, A. and WALTHER, J.H., "Discrete Vortex Simulation of Flow Around Five Generic Bridge Deck Sections", *J. Wind Eng. Ind. Aerodyn.*, Vol. 77 & 78, 1998, pp. 591-602.
- [4] LECHNER, B., *Aerodynamische Untersuchungen eines Modells der Hardangerbrücke im Windkanal des K+vif mit einer 5-Komponentenwaage*, K+vif, Graz, 2006.